ULTRASONIC RESPONSE IN Nd-Fe-B SINTERED MATERIAL DURING ELASTIC DEFORMATION

H. Ogi, M. Hirao, and A. Nozaki
Faculty of Engineering Science, Osaka University, Toyonaka
Osaka 560, Japan

INTRODUCTION

The rare earth material based on Nd-Fe-B alloy shows remarkable magnetic properties in the energy product $(BH)_{max}$ and coercive force. It is manufactured by pressing in a unidirectional magnetic field to align the easy axes, and then sintering, leading to a large magnetic and mechanical anisotropy between the normal and parallel directions. The material is first developed by Croat [1] and Sagawa [2] independently in 1984. Following them, many researchers [3-6] have studied the material. They concentrated the efforts on the investigation of the manufacturing process to have better magnetic properties as well as on the observation of the microstructure to understand the mechanism realizing the high coercive force. The previous studies showed that the material consists of the major phase of $Nd_2Fe_{14}B$ grains and the boundary phase of the Nd-rich alloys. It is considered that their different melting points and different thermal expansion coefficients introduce microcracks during the cooling process after sintering.

The material is now widely used as a high-performance permanent magnet, and it is formed not only in plates but in other shapes such as cylinder. Along with this, a nondestructive evaluation of stress and microcracks in the material is required because a large residual stress occurs in such a non-plate magnet due to the anisotropic thermal expansion coefficients [7]. However, to date, there is no study addressing nondestructive evaluation of the stress and microcracks.

The aim of this study is to develop a technique to continuously measure the ultrasonic velocity and attenuation in a sample with a noncontact way, and to investigate the fundamental behavior of the ultrasonic properties of the material to the applied stress. For the plate sample, we apply the compressive stress and continuously measure the velocities and attenuations of the two shear waves propagating in the thickness direction with the parallel and normal polarizations to the stress. The velocity and the attenuation are measured by the method of electromagnetic acoustic resonance (EMAR), which is capable of detecting the resonant frequency and the attenuation coefficient in high accuracy. The velocity change responding to the applied stress provides a means for the stress measurements. The attenuation response will help us to understand the microcracks in the material.

SAMPLES

The chemical composition is shown in Table I. The manufacturing process is as follows; (i) crushing the Nd-Fe-B alloy into powder of 3.5 μm-mean diameter, (ii) pressing the powder in a

Review of Progress in Quantitative Nondestructive Evaluation, Vol. 16
Edited by D.O. Thompson and D.E. Chimenti, Plenum Press, New York, 1997

Table.I Chemical Composition of Nd-Fe-B magnet (mass %)

Nd	B	Pr	Dy	Co	Nb	Fe
27.97	1.13	0.15	3.33	2.70	0.71	bal.

uniform magnetic field about 1 T, (iii) sintering it about 1000℃ for three hours in argon gas, and (iv) cooling it in argon gas to 80℃ in 4 hours.

We used four plate samples (*samples A* to *D*) to investigate the ultrasonic response to the compressive stress. They are 5 mm thick, 45 mm long, and 45 mm wide. They have different easy axes; *sample A* is manufactured without a magnetic field, having the randomly aligned easy axis. The easy axis of *sample B* is parallel to the thickness direction. For *sample C* and *sample D*, the axes are aligned in plane. We applied the compressive stress parallel to the easy axis of *sample C* and normal to that of *sample D*.

MEASUREMENT SYSTEM

Two shear-wave EMATs are located at the center of the sample surfaces as shown in Fig.1; one is for the shear wave polarized in the compressive stress direction, and the other is for the polarization normal to the stress direction. The EMAT has a permanent magnet block and the spiral elongated coil. The magnet is mounted on one side of the spiral coil, realizing the same probing area (8x8 mm^2) from both EMATs.

Figure 2 illustrates the measuring system. Two strain gauges are attached on the both sides of the sample for the measurement of the transverse strains to monitor the thickness change. We repeated the loading and unloading continuously at a frequency of 0.002 Hz up to a maximum load of 2 ton (~89 MPa). The system is capable of the continuous measurement of the thickness-resonant frequencies and the attenuation coefficients of the two shear waves at the same position

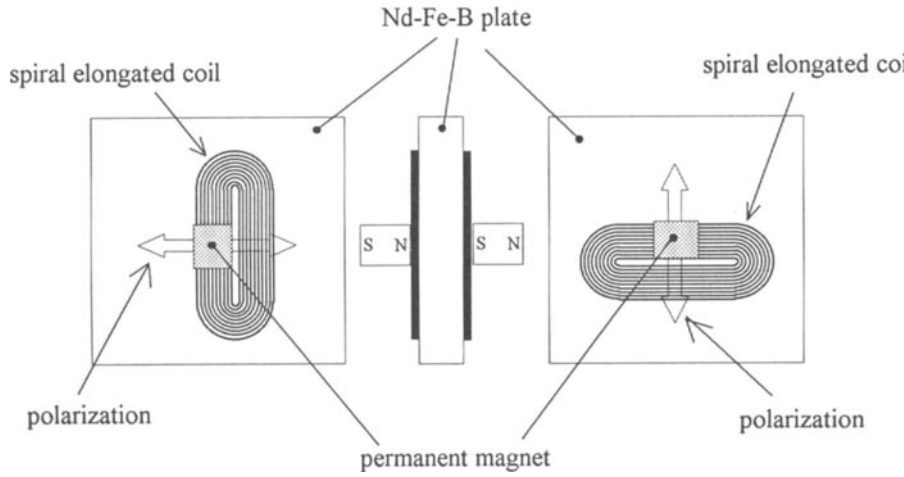

Figure.1 Measurement configuration of the two shear wave EMATs.

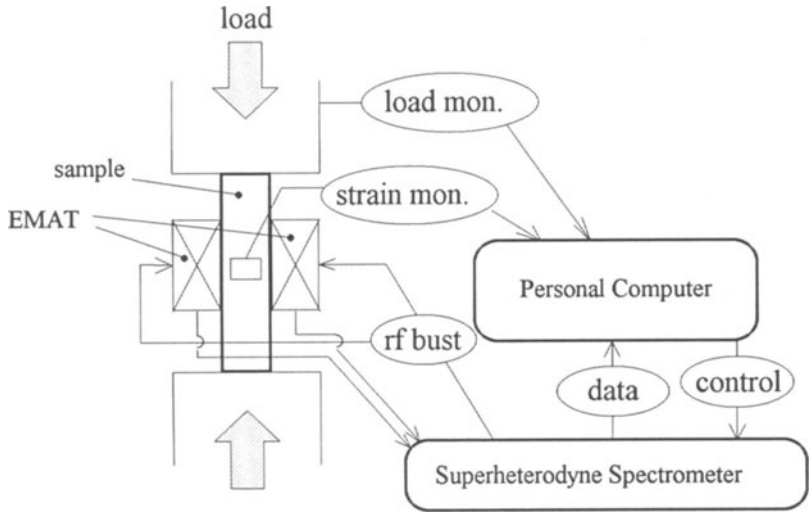

Figure.2 Measurement setup with two EMATs and superheterodyne spectrometer.

together with the transverse strains and the load at the same time. A resonant frequency is obtained by sweeping the frequency of the driving rf burst to the EMAT to obtain the resonant spectrum as shown in Fig.3 (a), and fitting the spectrum data around a resonant peak to a Lorentzian function, whose central axis gives the resonant frequency. The attenuation coefficient is measured by driving the EMAT with the measured resonant frequency, and then by sweeping a short integrator gate along the time axis to have the ringdown curve (Fig.3 (b)). We fit the ringdown curve to an exponential function and extract the time decay coefficient to determine the attenuation coefficient. The details of measuring operation can be found elsewhere [8]. From the thickness resonant frequency and the transverse strain, we calculate the shear wave velocity. We used the 17th-thickness resonant mode (~ 5MHz) throughout the present measurements.

RESULTS AND DISCUSSION

Figure 4 shows the velocity response to the applied stress observed with *sample A*. Both velocities of two polarizations increase with the compressive stress. In the first loading-unloading cycle, the velocities show hysteresis, but after that, no hysteresis is found.

The velocity responses observed in other samples were similar to that of *sample A*. The velocity changes are mainly caused by the acoustoelastic effect, which establishes the linear relation between the velocity and the stress, and is generally expressed as $c = c_0(1+C\sigma)$, where c is the velocity, σ the applied stress, c_0 the velocity at the stress-free condition, and C the acoustoelastic constant for the shear wave. Table II presents the acoustoelastic constants for the shear waves (C_S) and the birefringent-acoustoelastic constant (C_A), representing the slope of birefringence ($=2(c_1-c_2)/(c_1+c_2)$) to the stress; c_1 and c_2 are the shear wave velocities polarized parallel and normal to the principal stress. They are determined from the measurements excluding the hysteresis behavior for the initial loading. The absolute values of C_A are smaller than those of steels ($7\sim8 \times 10^{-6}$ MPa^{-1}). These can be used as fundamental data for the acoustoelastic stress measurement. The microcracks can also contribute to the velocity shift, but the effect is not so large in the present case as shown later.

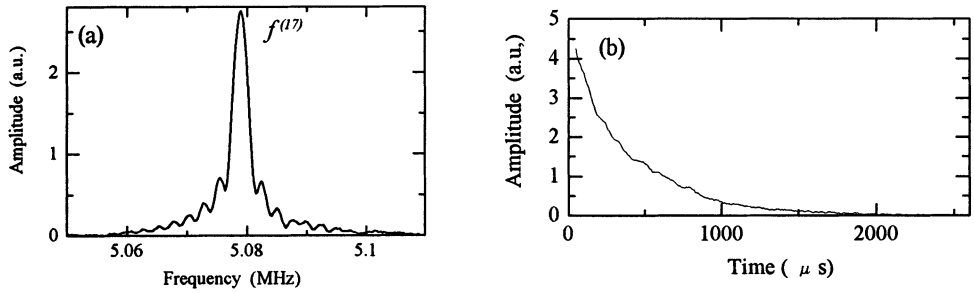

Figure.3 (a) Resonant spectrum and (b) ringdown curve observed in *sample A*.

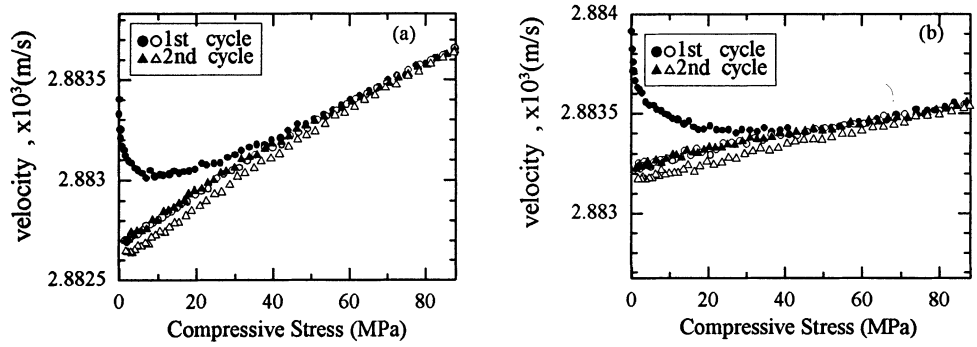

Figure 4. The velocity response in *sample A*. (a) Polarization in the stress direction and (b) polarization normal to the stress. Solid and open marks denote the data at loading and unloading sequences, respectively.

Table.II Acoustoelastic constants (x10^{-6} MPa^{-1}) of Nd-Fe-B plates. SD, MD, and PD indicate the stress direction, the easy axis-direction, and the propagation direction of the shear wave, respectively

	C_S (parallel)	C_S (normal)	C_A	condition
sample A	-3.97	-1.31	-2.66	SD⊥ PD
sample B	-3.57	-1.58	-1.99	SD⊥MD // PD
sample C	-3.46	-2.33	-1.13	SD⊥MD⊥PD
sample D	-4.58	-3.08	-1.50	SD // MD⊥PD

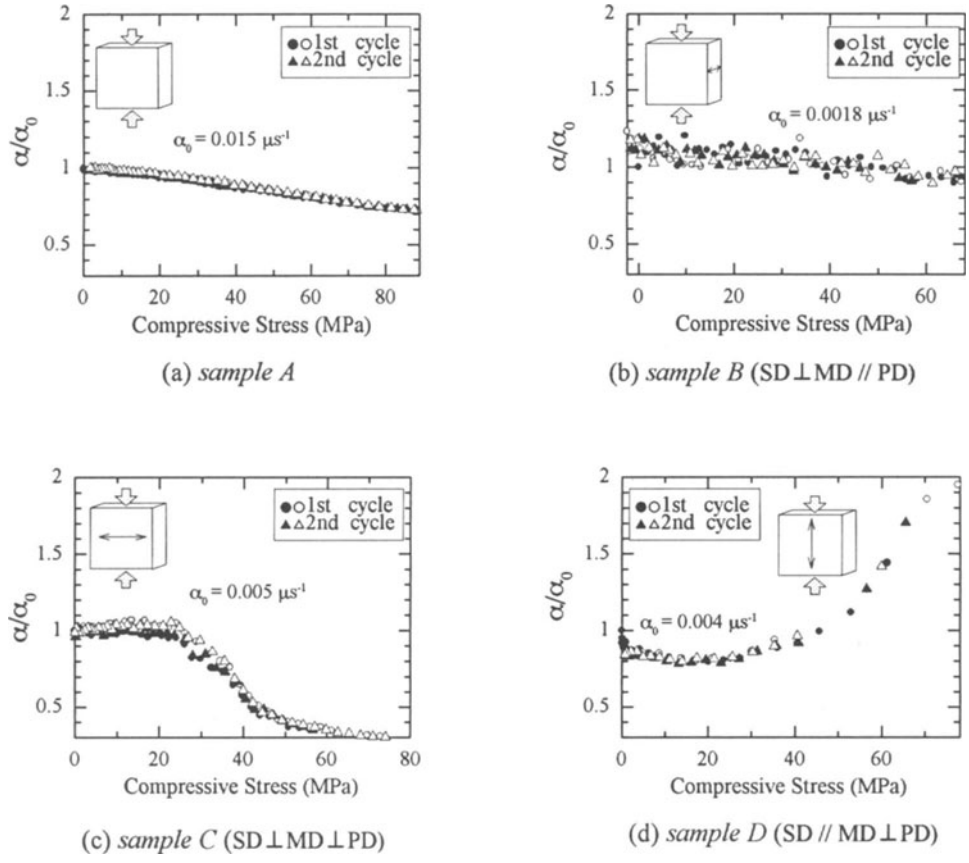

Figure 5. The attenuation response of the shear wave polarized in the stress direction. α_0 is the original attenuation coefficient. Solid and open marks indicate the data at loading and unloading sequences, respectively.

The attenuation response was almost independent of the shear wave polarization, and they did not show remarkable hysteresis change unlike the velocity. But, there were significant differences among the four geometries. Figure 5 shows the attenuation responses for the shear wave with the parallel polarization to the stress. From the results, we obtain the following observation; (i) the attenuation coefficient linearly decreases with the compressive stress for *sample A*, (ii) in *sample B*, the attenuation coefficient also decreases with the stress but both the original attenuation coefficient and the amount of their change are very small, and (iii) the attenuation coefficient considerably decreases in *sample C* but it increases in *sample D* as the stress increases.

These characters in the attenuation response can be explained by the closing and opening process of the microcracks in the material. The melting points and the thermal expansion coefficients of major phase of the $Nd_2Fe_{14}B$ grains and the binary boundary phase of the Nd-rich alloys are considerably different. This drives the crack occurrence at their boundaries in the cooling process after sintering. We make an assumption here that there are many microcracks elongated to the easy axis in the sample manufactured in a magnetic field as in Fig.6. In this model, the compressive stress applied parallel to the easy axis serves to open the microcracks, resulting in the increase of the attenuation due to the scattering, which is supported by the response in Fig.5 (d). The stress normal to the easy axis will close the crack faces and therefore it decreases the attenuation as shown in Figs.5 (b), (c). When propagating parallel to the easy axis, the ultrasonic wave is less scattered by the cracks, whether they are open or closed, because of the smaller scattering

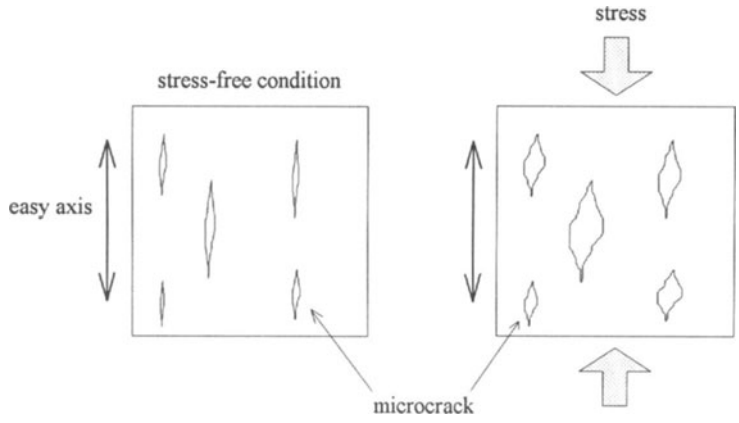

Figure 6. Model for the microcrack alignment to the easy axis.

cross section, leading to a small change in the attenuation coefficient and the smallest attenuation coefficient in *sample C*. In *sample A*, which was manufactured without applying the magnetic field, the crack faces are randomly orientated and they are closed by the compressive stress, resulting in the decrease of the attenuation (Fig.4 (a)). This interpretation is tentative. At present, we have no micrographs to support it, but this phenomenologically explains our results of the attenuation response.

Despite the large geometrical diversity among the four geometries in the attenuation response, apparently similar results in the velocity responses indicate that the effect of the microcracks on the velocity shift is small.

CONCLUSION

We have developed a system to continuously measure the velocities and attenuation coefficients of the two shear waves at the same position of the Nd-Fe-B plates. The shear wave velocities increased with the compressive stress for both parallel and normal polarization to the stress. In the initial loading-unloading cycle, the velocity changes displayed the hysteretic response, which were not observed in the attenuation response. From the velocity response to the stress, we calculated the acoustoelastic constants of the materials, which were smaller than those of common steels.

The attenuation coefficient showed various responses, depending on the stress direction and the easy axis. The attenuation response can be well explained by assuming the microcracks elongated in the easy axis along the dual phase boundaries.

REFERENCES

1. J. J. Croat, J. F. Herbst, R. W. Lee, and F. E. Pinkerton, J. Appl. Phys., **55**, 2078 (1984).
2. M. Sagawa, S. Fujimura, N. Togawa, and Y. Matsuura, J. Appl. Phys., **55**, 2083 (1984).
3. M. Sagawa, S. Fujimura, H. Yamamoto, Y. Matsuura, and K. Hiraga, IEEE Trans. Magn., **20**, 1584 (1984).
4. K. Miraga, M. Hirabayashi, M. Sagawa, and Y. Matsuura, Jpn. J. Appl. Phys., **24**, L30 (1985).
5. P. A. Withey, H. M. Kennett, P. Bowen and I. R. Harris, IEEE Trans. Magn., **26**, 2619 (1990).
6. K. Iwasaki, M. Shinoda, S. Tanigawa, and M. Tokunaga, IEEE Trans. Magn., **28**, 2850 (1992).
7. F. Kools, Science of Ceramics, **7**, 29 (1983).
8. H.Ogi, M.Hirao, and T.Honda, J. Acoust. Soc. Am., **98**, 458 (1995).